Band structure of a periodic quantum wire array

Yisong Zheng and Tsuneya Ando
Department of Physics, Tokyo Institute of Technology, 2-12-1 Ookayama, Meguro-ku, Tokyo 152-8551, Japan
(Received 1 May 2002; revised manuscript received 20 June 2002; published 29 August 2002)

The electron energy spectrum of a quantum-wire array consisting of an interface-corrugated quantum well is studied. It is calculated for actual structures with periodic well-width variation by the numerical diagonalization of the Hamiltonian matrix. Then a one-dimensional effective-potential model is developed, which can reproduce the energy spectrum almost exactly even when the quantum well becomes very thin. A self-consistent calculation shows that the Coulomb potential has only a trivial influence on the band structure. In the absence of a magnetic field, the subband structure, Fermi surface geometry, density of states, and the cyclotron effective mass are obtained. In a high magnetic field a magnetic miniband structure is present but its width is negligibly small near the Fermi level in systems currently accessible experimentally.

DOI: 10.1103/PhysRevB.66.085328 PACS number(s): 73.21.Hb, 73.21.Fg, 73.21.Cd, 73.21.Ac

I. INTRODUCTION

Recently, a periodic quantum-wire array (QWA) was formed during growth of a GaAs/AlAs heterointerface on a GaAs (775)B substrate by molecular beam epitaxy.[1–5] Under suitable growth conditions, a zigzag heterointerface comes into being instead of a flat plane. The periodic unit cell of this QWA is illustrated in Fig. 1. It is considered as an ideal structure for the study of transport properties of the periodically modulated two-dimensional (2D) electron gas, since it possesses a good interface quality and a period much shorter than conventional lateral superlattices. Transport experiments were started quite recently.[5,6] The purpose of this paper is to calculate the subband structure of such QWA systems.

The spatial modulation of the heterointerface gives rise to an additional subband structure which provides the possibility that electronic properties differ from those of a uniform 2D system. Therefore, a quantitative knowledge on the subband structure of such systems is highly desirable. In the present paper, we calculate the electron energy spectra of QWA's by a numerical diagonalization of the Hamiltonian matrix in both cases with and without a magnetic field. In addition, we establish a 1D effective potential which can reproduce the electron energy spectrum. On the basis of this model electronic states can be understood more intuitively.

The paper is organized as follows: In Sec. II the formulation to calculate the subband structure is described and a 1D effective-potential model is developed to simulate the periodic variation of the well width. In Sec. III the numerical results are presented. Some discussion on relevant experiments is given in Sec. IV. In Sec. V the main results are summarized.

II. FORMULATION

A. Case without magnetic field

The periodic unit cell of a QWA is illustrated in Fig. 1, where the structure parameters used in the calculation are described. The z axis is chosen in the direction of the growth direction, and the well width varies in the x direction and is independent of the y coordinate. The single-electron Hamiltonian in the effective-mass approximation is written as

$$H=\frac{\hat{\boldsymbol{p}}^2}{2m^*}+V(x,z), \tag{1}$$

where $\hat{\boldsymbol{p}}=-i\hbar\vec{\nabla}$, m^* is the effective mass of the bulk material comprising a QWA (GaAs in the present case), and we ignore the mismatch of the effective mass between the well and barrier materials. The periodic potential in the region $0\leqslant x<a$ and $0\leqslant z<d$ is given by

$$V(x,z)=V_0\{\theta(-z)+\theta[z-w(x)]\}, \tag{2}$$

with

$$w(x)=\begin{cases} d_1+\Delta\dfrac{x}{a_1}, & 0\leqslant x<a_1 \\ d_1+\Delta\dfrac{a-x}{a_2}, & a_1\leqslant x<a, \end{cases} \tag{3}$$

where $\theta(t)=1$ for $t\geqslant 0$ and 0 for $t<0$, and a and d are the period in the x and z directions, respectively.

The wave function for the electron motion along the y direction is given by a plane wave $e^{iq_y y}/\sqrt{L_y}$, where q_y is the

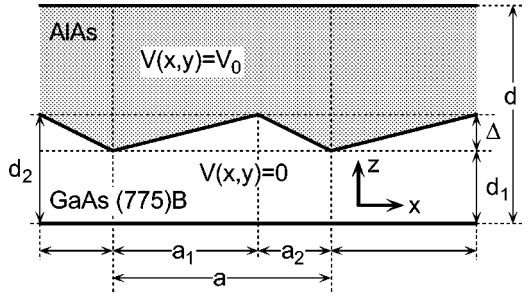

FIG. 1. A schematic illustration of a periodic unit cell of QWA's consisting of a GaAs/AlAs heterostructure. The structure parameters concerned are explained graphically. The quantum wires are along the y direction.

wave vector and L_y is the linear dimension in the y direction. Thus the Schrödinger equation and the energy spectrum can be expressed as

$$\left[\frac{1}{2m^*}(\hat{p}_x^2+\hat{p}_z^2)+V(x,z)\right]\psi_{k_x,k_z}(x,z)=\varepsilon_n(k_x)\psi_{k_x,k_z}(x,z) \tag{4}$$

and

$$E_n(k_x,q_y)=\varepsilon_n(k_x)+\frac{\hbar^2 q_y^2}{2m^*}, \tag{5}$$

where $\varepsilon_n(k_x)$ is the subband energy with n denoting the subband index. The wave vector k_x is confined in the first Brillouin zone, i.e., $-\pi/a \leqslant k_x < \pi/a$. In the following we take a large value for d depending on the barrier height to eliminate coupling between adjacent wells and choose $k_z=0$.

The wave function can be expanded in terms of a set of plane waves as

$$\psi_{k_x,k_z}(x,z)=\sum_{n_x,n_z} C_{n_x,n_z}(k_x,k_z)|n_x,k_x;n_z,k_z\rangle, \tag{6}$$

with

$$|n_x,k_x;n_z,k_z\rangle=\frac{1}{\sqrt{L_x}}\exp\left[i\left(k_x+\frac{2\pi n_x}{a}\right)x\right] \times\frac{1}{\sqrt{L_z}}\exp\left[i\left(k_z+\frac{2\pi n_z}{d}\right)z\right], \tag{7}$$

where n_x and n_z are arbitrary integers, and L_x and L_z are the linear dimension in the x and z direction, respectively.

The Hamiltonian matrix element is given by

$$\begin{aligned}&\langle n_x',k_x';n_z',k_z'|H|n_x,k_x;n_z,k_z\rangle \\ &=\frac{\hbar^2}{2m^*}\left[\left(k_x+\frac{2\pi n_x}{a}\right)^2+\left(k_z+\frac{2\pi n_z}{d}\right)^2\right]\delta_{n_x,n_x'}\delta_{n_z,n_z'} \\ &\times\delta_{k_x,k_x'}\delta_{k_z,k_z'}+\mathcal{V}(n_x-n_x',n_z-n_z')\delta_{k_x,k_x'}\delta_{k_z,k_z'},\end{aligned} \tag{8}$$

with

$$V(x,z)=\sum_{n_x,n_z}\mathcal{V}(n_x,n_z)\exp\left(i\frac{2\pi n_x}{a}x+i\frac{2\pi n_z}{d}z\right). \tag{9}$$

It can be seen that the Hamiltonian is diagonal with respect to k_x and k_z. The matrix element of the potential takes different forms according to the following cases: (i) When $m\neq 0$,

$$\begin{aligned}\mathcal{V}(n,m)=&-\frac{V_0}{2\pi i m}\left\{\delta_{n0}-\frac{1}{2\pi i}\exp\left(-\frac{2\pi i m d_1}{d}\right)\right. \\ &\times\left[1-\exp\left[-2\pi i\left(\frac{a_1}{a}n+\frac{\Delta}{d}m\right)\right]\right]\left[\left(n+\frac{a\Delta}{a_1 d}m\right)^{-1}\right. \\ &\left.\left.-\left(n-\frac{a\Delta}{a_2 d}m\right)^{-1}\right]\right\}.\end{aligned} \tag{10}$$

(ii) When $m=0$ and $n\neq 0$,

$$\mathcal{V}(n,0)=V_0\frac{\Delta}{d}\left(\frac{1}{2\pi n}\right)^2\frac{a^2}{a_1 a_2}\left[1-\exp\left(-\frac{2\pi i n a_1}{a}\right)\right]. \tag{11}$$

(iii) When $n=m=0$,

$$\mathcal{V}(0,0)=\frac{V_0}{d}\left(d-d_1-\frac{\Delta}{2}\right). \tag{12}$$

In the simplest Hartree approximation, the influence of the Coulomb potential of electrons themselves can be taken into account by incorporating the following term in the Hamiltonian:

$$V_c(\boldsymbol{r})=\int\frac{\rho(\boldsymbol{r}')}{\epsilon|\mathbf{r}-\mathbf{r}'|}d\mathbf{r}', \tag{13}$$

where ϵ is the dielectric constant of the GaAs material. The local electron density $\rho(\boldsymbol{r})$ at the position $\boldsymbol{r}=(x,y,z)$ is given by

$$\rho(\boldsymbol{r})=\sum_n\sum_{q_y}\sum_{k_x,k_z}2|\psi_{k_x,k_z}(x,z)|^2\theta[E_F-E_n(k_x,q_y)], \tag{14}$$

where E_F is the Fermi energy, and the factor 2 denotes the spin degeneracy. Then the matrix element of the Coulomb potential takes the form

$$\mathcal{V}_c(\boldsymbol{G})=\frac{4\pi e^2}{\epsilon G^2}\tilde{\rho}(\boldsymbol{G}), \tag{15}$$

where $\boldsymbol{G}$ is the 2D reciprocal-lattice vector and the component $\boldsymbol{G}=0$ should be excluded in Eq. (15) since it cancels the potential of the uniform positive charge background exactly in the case of uniform doping. The Fourier components $\tilde{\rho}(\boldsymbol{G})$ can be extracted from Eq. (14) if the plane-wave expansion of the wave function is substituted into it. Thus the subband structure can be calculated self-consistently.

We can work out the density of states from the resulting subband structure. From the primary definition of the density of states,

$$D(\varepsilon)=\frac{2}{L_x L_y}\sum_n\sum_{k_x,q_y}\delta[\varepsilon-E_n(k_x,q_y)], \tag{16}$$

through a straightforward evaluation, we have

$$D(\varepsilon)=\sqrt{\frac{2m^*}{2\pi^2\hbar}}\sum_n\int dk_x\frac{\theta[\varepsilon-\varepsilon_n(k_x)]}{\sqrt{\varepsilon-\varepsilon_n(k_x)}}, \tag{17}$$

where the spin degeneracy is included. In addition, it can readily be proved that the cyclotron effective mass m_c^* is associated with the density of states through

$$m_c^*=\pi\hbar^2 D(\varepsilon). \tag{18}$$

B. Case in a magnetic field

When a magnetic field $\boldsymbol{B}$ is applied along the z direction, i.e., $\boldsymbol{B}=(0,0,B)$, the single electron Hamiltonian has the same form as Eq. (1) except that the momentum operator $\hat{\boldsymbol{p}}$ is replaced by $\hat{\boldsymbol{p}}+e\boldsymbol{A}/c$, with $\boldsymbol{A}=(0,Bx,0)$ in the Landau gauge. When the periodic potential $V(x,z)$ is absent, the eigenenergy and the wave function are given as

$$E_n^0(q_z)=\left(n+\frac{1}{2}\right)\hbar\omega_c+\frac{\hbar^2 q_z^2}{2m^*} \tag{19}$$

and

$$\psi_{n,q_y,q_z}(\boldsymbol{r})=\frac{1}{\sqrt{L_y L_z}}\exp(iq_y y+iq_z z)\,\phi_n(x+l_0^2 q_y), \tag{20}$$

with

$$\phi_n(x+l_0^2 q_y)=\frac{1}{\sqrt{2^n n!\, l_0\sqrt{\pi}}}\exp[-(x+l_0^2 q_y)^2/2l_0^2]\times H_n[(x+l_0^2 q_y)/l_0], \tag{21}$$

where the magnetic length is defined as $l_0=\sqrt{\hbar c/eB}$, the cyclotron frequency is $\omega_c=eB/m^*c$, and $H_n(t)$ is the Hermite polynomial.

When the periodic potential $V(x,z)$ is incorporated, the wave vector q_z should be folded into the Brillouin zone by a relation like $q_z=k_z+2m\pi/d$. Thus the wave function shown by Eq. (20) can be denoted as $|n,q_y;m,k_z\rangle$, which is employed as the basis set for the expansion in the presence of a magnetic field. Then the Hamiltonian matrix can be expressed as

$$\begin{aligned}\langle n',q_y';m',k_z'|H|n,q_y;m,k_z\rangle &= E_n^0(q_z)\,\delta_{nn'}\delta_{q_y q_y'}\delta_{mm'}\delta_{k_z k_z'}\\ &\quad+\langle n',q_y';m',k_z'|V(x,z)|n,q_y;m,k_z\rangle\,\delta_{q_y q_y'}\delta_{k_z k_z'}.\end{aligned} \tag{22}$$

It can be seen that the Hamiltonian matrix is diagonal with respect to q_y and k_z. The matrix element of the potential can be calculated by the following integral:

$$\begin{aligned}&\langle n',q_y;m',k_z|V(x,z)|n,q_y;m,k_z\rangle\\ &\quad=\int_{-\infty}^{\infty}dx\,\phi_n(x+l_0^2 q_y)\,\phi_{n'}(x+l_0^2 q_y)\\ &\qquad\times\frac{1}{d}\int_0^d dz\exp\left[i(m-m')\frac{2\pi}{d}z\right]V(x,z).\end{aligned} \tag{23}$$

Because of the periodicity of the potential $V(x,z)$, it can be deduced that the second integral on the right side of Eq. (23) gives a periodic function of x with period of a. With this result, for a fixed magnetic field B it can be readily found that two different states with wave vectors q_y and q_y', satisfying $l_0^2 q_y=l_0^2 q_y'+Na$ with N an arbitrary integer, possess the same matrix element of the potential. Therefore, the eigen energy is a periodic function of wave vector q_y, i.e.,

$$E_n(q_y)=E_n(q_y+Na/l_0^2). \tag{24}$$

The period a/l_0^2 is dependent on the magnetic field, and therefore the band structure in a magnetic field is called the magnetic miniband. By using Fourier expansion (9), the matrix element of the potential is evaluated as[7]

$$\begin{aligned}&\langle n',q_y;n_z',k_z|V(x,z)|n,q_y;n_z,k_z\rangle\\ &\quad=\sum_{n_x}\mathcal{V}(n_x,n_z'-n_z)J_{nn'}\left(\frac{2\pi n_x}{a},l_0^2 q_y\right),\end{aligned} \tag{25}$$

with

$$\begin{aligned}J_{nn'}(G,t)&=\exp\left[-iGt-\left(\frac{l_0 G}{2}\right)^2\right]\left(i\frac{l_0 G}{\sqrt{2}}\right)^{n_1-n_2}\left(\frac{n_2!}{n_1!}\right)^{1/2}\\ &\quad\times L_{n_2}^{(n_1-n_2)}\left[\frac{(l_0 G)^2}{2}\right],\end{aligned} \tag{26}$$

where $n_1=\max(n,n')$, $n_2=\min(n,n')$, and $L_n^{(r)}(t)$ is the associated Laguerre polynomial.

It is well known that the Coulomb interaction plays an essential role in the magnetotransport of a 2D system in high magnetic fields, and leads to the fractional quantum Hall effect. In quantum wires, a self-consistency between the electron density distribution and the potential is known to sometimes lead to the formation of compressible and incompressible strips.[8–10] This strip formation is quite sensitive to the detail of the confinement potential and also to temperature.[11] The self-consistent calculation in such high magnetic fields is out of the scope of this paper and will be left for a future study.

C. One-dimensional effective-potential model

In the following we establish a one-dimensional effective-potential model to simulate the energy spectrum by treating the periodic well-width variation in a manner similar to that of interface roughness.[12,13] The periodic potential can be expressed as

$$V(x,z)=V_0\,\theta[-z]+V_0\,\theta\{z-d'-[w(x)-d']\}, \tag{27}$$

where d' is the average width of a quantum well given by

$$d'=\frac{1}{2}(d_1+d_2). \tag{28}$$

When $w(x)-d'$ is smaller than d', we can expand the second term of the right side of Eq. (27) in terms of $w(x)-d'$ and only retain the linear term. Then we obtain an approximate expression of the periodic potential as

$$V(x,z)\approx V_0\theta(-z)+V_0\theta(z-d')-V_0\delta(z-d')[w(x)-d']. \tag{29}$$

Then the one-dimensional effective potential takes the form

$$V_{\rm eff}(x)=-V_0|\xi(d')|^2[w(x)-d'], \tag{30}$$

where $\xi(z)$ is the wave function of the quantum-well ground state, given by

$$\xi(z)=\begin{cases} B_0\cos(Qz'), & |z'|\leqslant\dfrac{d'}{2} \\ B_0\cos\left(\dfrac{Qd'}{2}\right)\exp\left[-Q'\left(\left|z'\right|-\dfrac{d'}{2}\right)\right], & |z'|>\dfrac{d'}{2}, \end{cases} \tag{31}$$

with $z'=z-d'/2$ and

$$B_0=\left[\frac{2Q}{Qd'+\sin(Qd')+(2Q/Q')\cos^2(Qd'/2)}\right]^{1/2},$$

$$Q=\sqrt{\frac{2m^*\varepsilon_z}{\hbar^2}},\quad Q'=\sqrt{\frac{2m^*(V_0-\varepsilon_z)}{\hbar^2}}. \tag{32}$$

The ground state energy of the quantum well ε_z is determined by

$$\tan\left(Q\frac{d'}{2}\right)=\left[\frac{V_0-\varepsilon_z}{\varepsilon_z}\right]^{1/2}. \tag{33}$$

Finally the effective potential evolves into

$$V_{\rm eff}(x)=-V_0B_0^2\cos^2\left(\frac{Qd'}{2}\right)[w(x)-d']. \tag{34}$$

This 1D effective potential possesses a linear dependence on the x coordinate as is clear in the above equation. It has the maxima at $x=x_1$ with $w(x_1)=d_1$ and the minima at $x=x_2$ with $w(x_2)=d_2$. The amplitude of the potential becomes

$$\Delta V\equiv V_{\rm eff}(x_1)-V_{\rm eff}(x_2)=V_0B_0^2\Delta\cos^2\left(\frac{Qd'}{2}\right). \tag{35}$$

Now we have separated the electron motion into three parts; freely moving along the y direction, confined in a quantum well with width d' in the z direction, and moving along the x direction subject to the effective potential. Then the energy spectrum can be expressed as

$$E_n(k_x,q_y)=\varepsilon_z+\frac{\hbar^2q_y^2}{2m^*}+\varepsilon_n(k_x), \tag{36}$$

where $\varepsilon_n(k_x)$ is the one-dimensional energy spectrum of the effective-potential model along the x direction. It will be demonstrated in Sec. III that the model can reproduce the electron energy spectrum almost exactly even when the quantum well becomes very thin.

In the limit of an infinitely high barrier, i.e., $V_0\to\infty$, we have $B_0\approx\sqrt{2/d'}$ and $\cos(Qd'/2)\approx\sqrt{\varepsilon_z/V_0}$ with $\varepsilon_z\approx\pi^2\hbar^2/2m^*d'^2$. Therefore, we have

$$V_{\rm eff}(x)=-\frac{\hbar^2}{2m^*}\left(\frac{\pi}{d'}\right)^2\frac{2}{d'}[w(x)-d']. \tag{37}$$

In the case of an infinite-potential well, for a fixed x the energy of the electron motion in the z direction is simply given by

$$\varepsilon_z[w(x)]=\frac{\hbar^2}{2m^*}\left(\frac{\pi}{w(x)}\right)^2. \tag{38}$$

By expanding Eq. (38) with respect to $w(x)-d'$ and just retaining the linear term, we can obtain Eq. (37), as expected. We shall see in the following that this infinite-potential approximation is very poor in the present GaAs/AlAs system.

D. Numerical calculation

In accordance with a typical experimental sample,[6] we take the values of the structure parameters as $a=12$ nm, $a_1=4$ nm, and $\Delta=1.2$ nm, and use two typical values $d_1=5$ and 2 nm for the well thickness. The band offset is chosen as $V_0=1$ eV at the Γ point for the GaAs/AlAs heterostructure.[14,16,17] The superlattice period is chosen as $d=20$ nm, for which the energy becomes independent of k_z. The dielectric constant and the effective mass take the values of the GaAs material $\epsilon=13$ and $m^*=0.067m_e$ where m_e is the free-electron mass.[18] In actual numerical calculations the Hamiltonian matrix is truncated at $|n_x|\leqslant10$ and $|n_z|\leqslant20$ in the absence of a magnetic field and $0\leqslant n\leqslant50$ and $|m|\leqslant20$ in the presence of a magnetic field, by which the steady numerical results are guaranteed. In a magnetic field the spin splitting is completely neglected because it only gives a very small splitting to the energy spectrum.[19]

III. NUMERICAL RESULTS

A. Subband in the absence of a magnetic field

In Fig. 2 the calculated lowest two subbands are shown as a function of k_x for both cases of $d_1=5$ and 2 nm. The parabolic dispersion relation of the free electron motion, folded into the Brillouin zone, is also plotted for comparison. It can be seen that the subband structure deviates from the parabolic dispersion when k_x approaches the boundary of the Brillouin zone, where a band gap is formed. Such a feature is exhibited more remarkably in the case of $d_1=2$ nm, because of the relatively stronger modulation of the periodic potential than the case of $d_1=5$ nm. The Fermi energies denoted by the horizontal lines correspond to a typical experimental value of the electron number density[6] $n_e=3.9\times10^{11}$ cm^{-2}. It can be seen that only the first subband is partially occupied and only in the case of $d_1=2$ nm the subband structure deviates from the parabolic dispersion significantly around the Fermi level.

In Fig. 3 the density of states is shown in the energy range covering two lowest subbands. The sharp peaks indicate the

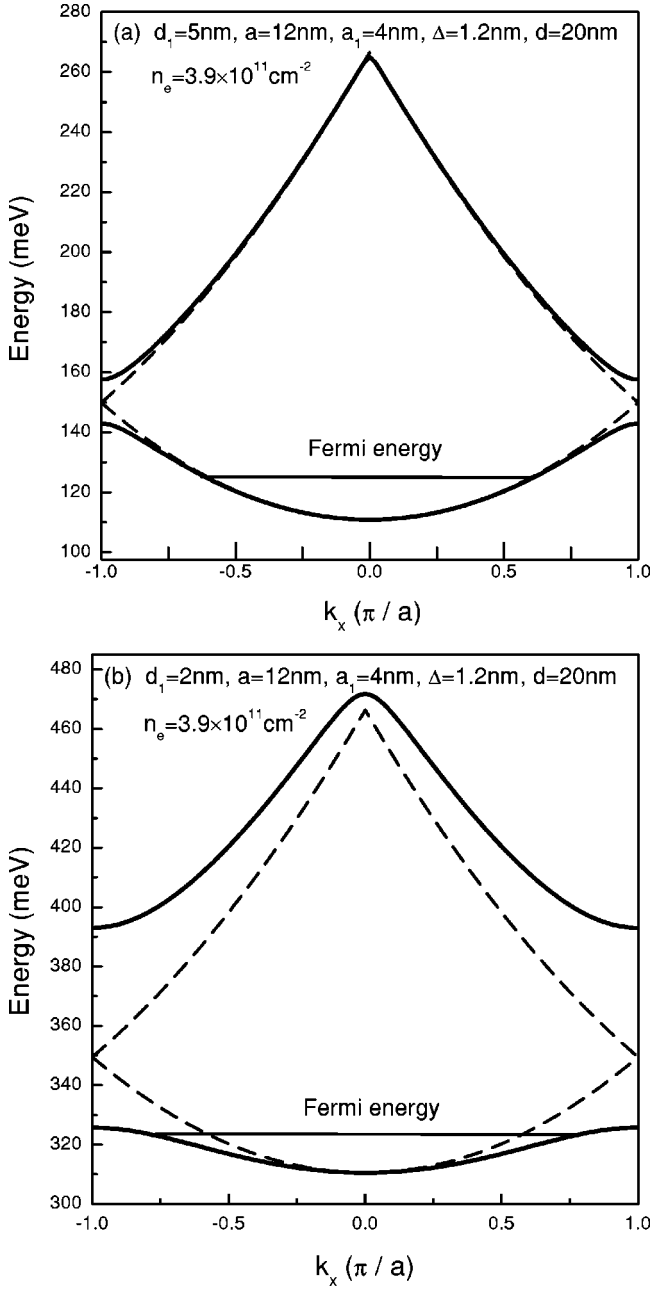

FIG. 2. The two lowest subbands as functions of the wave vector k_x for (a) $d_1=5$ nm and (b) $d_1=2$ nm. The parabolic dispersion relation for the free electron, folded into the Brillouin zone, is shown by dashed lines for comparison. The Fermi energy position denoted by the horizontal lines corresponds to $n_e=3.9\times10^{11}$ cm^{-2}.

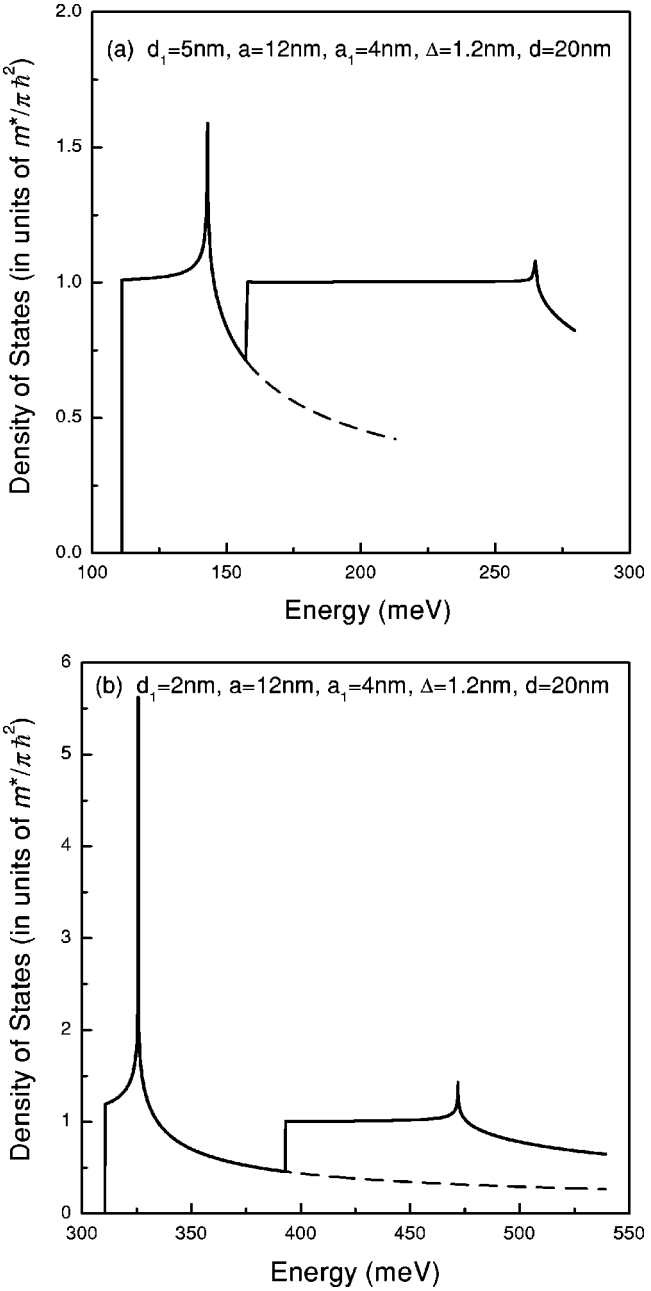

FIG. 3. The density of states for (a) $d_1=5$ nm and (b) $d_1=2$ nm, in units of $m^*/\pi\hbar^2$, the density of states in a uniform 2D system. The solid lines show the result in which the contributions of the two lowest subbands are taken into account and the dashed lines that in which only the contribution of the first subband is included.

Van Hove singularities at $k_x=\pm\pi/a$ and $q_y=0$ in the first subband and $k_x=0$ and $q_y=0$ in the second subband. In the case of $d_1=5$ nm, the density of states agrees with $m^*/\pi\hbar^2$ very well almost in the whole energy range. A notable deviation is present in the case of $d_1=2$ nm, especially in the energy range of the first subband, which is consistent with the subband structure shown in Fig. 2. The dashed lines show the density of states with only the contribution of the first subband included. When the energy exceeds the position of the first peak, the first subband is fully occupied and the corresponding density of states has a 1D behavior as decreases with the energy.

Figure 4 shows the Fermi lines corresponding to $n_e=3.9\times10^{11}$ cm^{-2}. The Fermi energies are 125 meV (14 meV measured from the bottom of the subband at 111 meV) in the case of $d_1=5$ nm and 322 meV (11 meV measured from the bottom of the subband at 311 meV) in the case of $d_1=2$ nm. The circular Fermi lines of the uniform 2D system are also shown for comparison. The difference is significant only in the case of $d_1=2$.

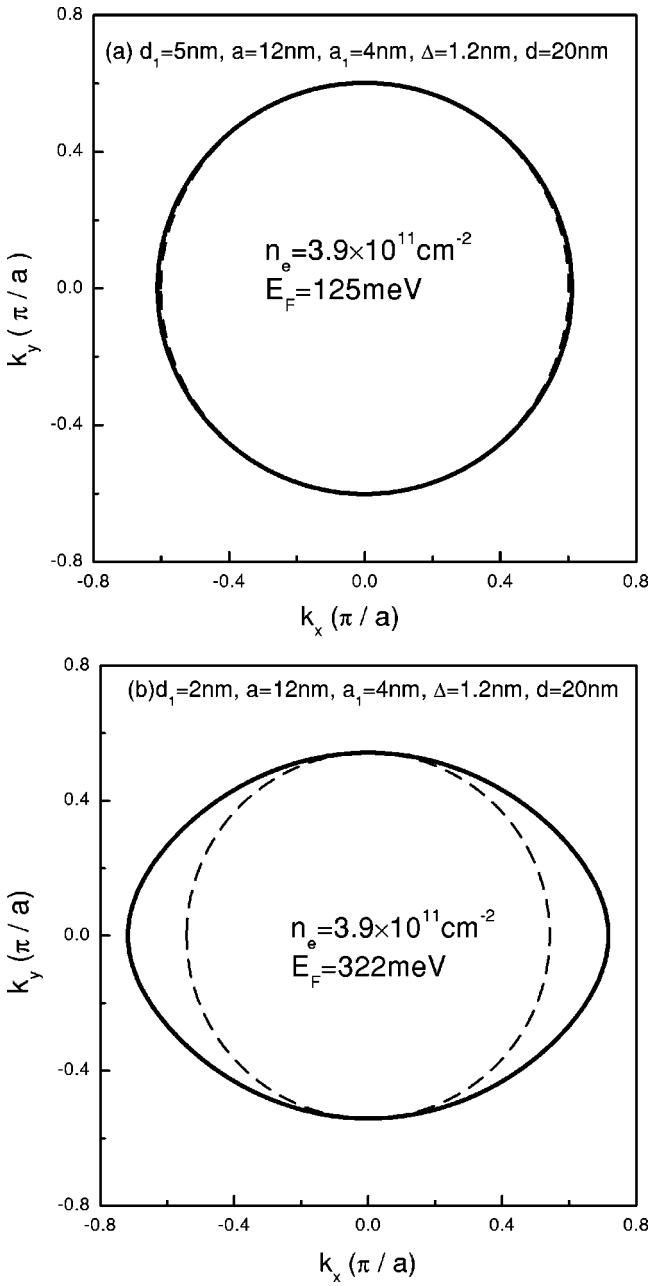

FIG. 4. The Fermi line (solid lines) with the Fermi energy and d_1 equal to (a) 125 meV and 5 nm and (b) 322 meV and 2 nm, respectively. The dashed lines show the circular Fermi line of the uniform 2D system for the same Fermi energy.

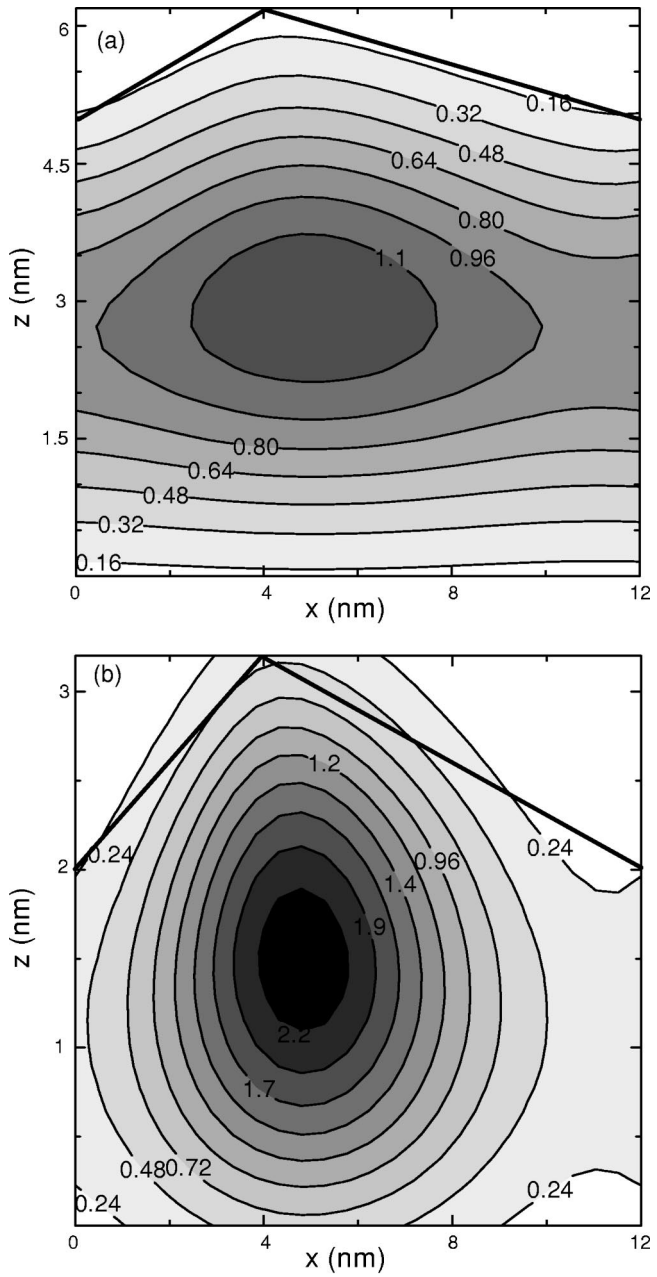

FIG. 5. The local electron density for (a) $d_1=5$ nm and (b) $d_1=2$ nm in units of 10^{18} cm^{-3}. The other parameters take the values as $a=12$ nm, $a_1=4$ nm, $\Delta=1.2$ nm, $d=20$ nm, and $n_e=3.9\times10^{11}$ cm^{-2}. The thick straight lines in the upper region denote the corrugated interface.

B. Hartree potential

Figure 5 shows examples of local electron density obtained self-consistently for $n_e=3.9\times10^{11}$ cm^{-2}. For a uniform quantum well, the density is independent of the x coordinate and its maximum occurs at the center of the quantum well if only the lowest subband is occupied. From Fig. 5(a) we can see that such a feature remains approximately except for a weak localization in the wide quantum-well region for the case of $d_1=5$ nm. On the other hand, in Fig. 5(b) the density shows notable spatial variation along the x direction in the case of $d_1=2$ nm.

Figure 6 shows a comparison of the subband structure with and without the Coulomb potential incorporated [the energy origin is chosen at the bottom of the conduction band at $\boldsymbol{r}=(0,0,0)$ in Fig. 1]. It can be found that the Coulomb potential gives rise to a small parallel shift of the subbands as well as a trivial correction on the subband gap ($\sim5\%$). This is true even in the case of $d_1=2$ nm for which the density shows a strong localization as shown in Fig. 5(b). Therefore, the Coulomb potential can be ignored in the calculation of the subband structure in the range of the electron density accessible experimentally.

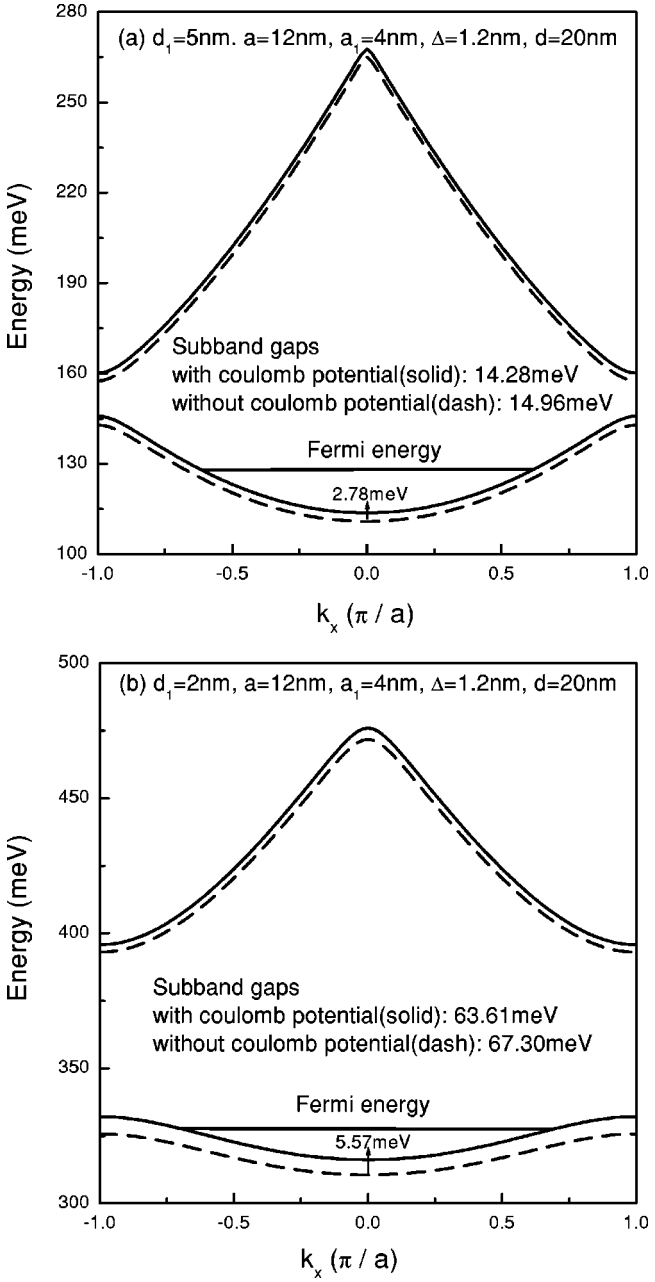

FIG. 6. A comparison of the subband structure between the case in which the electron Coulomb potential is included (solid lines) self-consistently and that in which it is excluded (dashed lines) for (a) $d_1=5$ nm and (b) $d_1=2$ nm. The origin of the energy is chosen at the conduction-band bottom of GaAs at $\boldsymbol{r}=0$. The numbers near the subband bottoms denote the subband shifts.

C. Subband in a magnetic field

Figure 7 shows the calculated magnetic miniband structure as a function of q_y for $d_1=5$ nm. Figure 7(a) shows that the miniband width is negligible for levels in the vicinity of the Fermi energy in a weak magnetic field of $\hbar\omega_c=5$ meV. It can be found that the width of the magnetic miniband is so small that it cannot be observed. When the magnetic field increases to $\hbar\omega_c=10$ meV and further to 20 meV, the magnetic-miniband characteristic comes into being notably, as shown by Figs. 7(b) and 7(c), but the width of the miniband at the Fermi level remains almost negligible. In the case of $d_1=2$ nm the miniband width at the Fermi level becomes quite remarkable as shown in Fig. 7(d).

From Fig. 2 we can find that the lowest Landau levels are located at the vicinity of the bottom of the first subband where the modulation of the periodic potential does not play an important role and the electron motion is described by the simple parabolic dispersion relation. Consequently, the broadening is extremely small in the lowest magnetic miniband. Contrarily, at positions of higher Landau levels, where significant deviation of the subband structure from the parabolicity occurs, the modulation gives rise to notable magnetic-miniband broadening.

The magnetic minibands have a 1D characteristic, which is manifested by singularities of the density of states as shown in Fig. 8. Because the Landau-level picture is not wholly destroyed, the occupation of the magnetic minibands can be estimated by the degeneracy of the individual Landau level of the uniform 2D system. Each Landau level possesses the degeneracy of $1/2\pi l_0^2$; thereby we can estimate, for example, that the first miniband is totally occupied and the second miniband is partially occupied for $n_e=3.9\times10^{11}$ cm^{-2} in the field given by $\hbar\omega_c=10$ meV.

D. One-dimensional effective potential

In Fig. 9 the amplitude of the 1D effective potential ΔV defined in Eq. (35) is shown as a function of d_1 for cases of both finite and infinite barriers. They are quite different when $d_1\leqslant5$ nm, which implies that the infinite-barrier model is still inappropriate even for $V_0=1$ eV in the present GaAs/AlAs QWA.

Our calculation indicates that the finite-barrier effective potential model can reproduce the electron spectra almost exactly both in the presence and absence of a magnetic field, except for a slight parallel shift which can safely be ignored. In Fig. 9 a comparison is made for the subband gap between the first and second subbands calculated by different schemes. It can be found that the gap calculated by the effective potential agrees with the exact one very well, even when the parameter d_1 becomes as small as 2 nm.

Figure 10 shows the gap as a function of V_0 obtained by using different schemes. The effective potential works quite well in the whole range of V_0. With the decrease of V_0 the gap becomes smaller rapidly. This implies that the deviation of the subband structure from parabolic dispersion relation is negligible in GaAs/Al_xGa_{1-x}As quantum-wire arrays independent of the Al concentration x except in systems with very high electron concentrations.

IV. DISCUSSION

The experimental measurement about the diagonal resistivity showed that the minima corresponding to the odd filling factors $\nu=3$ and 5 are invisible and the resistance dip around $\nu=1$ quickly disappears as temperature increases from 40 mK to about 300 mK,[6] where $\nu=2\pi l_0^2 n_e$. The dip in the resistivity at odd-integer fillings corresponds to the

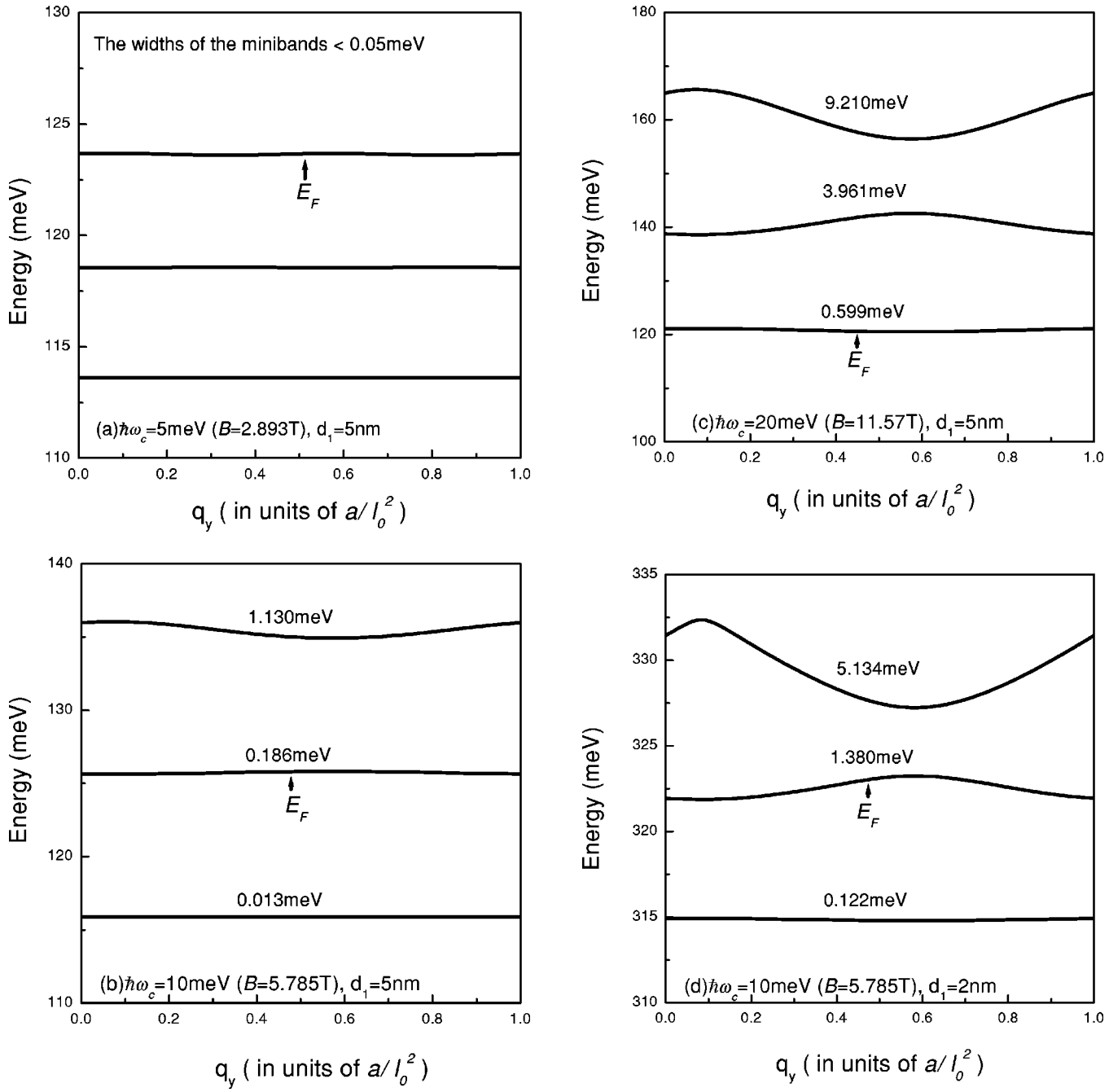

FIG. 7. The magnetic minibands as a function of the wave vector q_y for several cases. (a) $\hbar\omega_c=5$ meV, $B=2.893$ T, and $d_1=5$ nm; (b) $\hbar\omega_c=10$ meV, $B=5.785$ T, and $d_1=5$ nm; (c) $\hbar\omega_c=20$ meV, $B=11.57$ T, and $d_1=5$ nm; and (d) $\hbar\omega_c=10$ meV, $B=5.785$ T, and $d_1=2$ nm. The numbers near the minibands denote their widths, and the Fermi level is denoted by arrows.

spin splitting, which has completely been ignored in the present calculation.

In the uniform 2D system the exchange energy is known to lead to a drastic enhancement of spin splitting, which makes the diagonal resistance minima of odd fillings visible as well as those of even fillings.[20] The spin gap due to the exchange enhancement effect is suppressed when the degeneracy of the Landau levels is lifted by a periodic modulation potential.[21] In the QWA structure, the periodically modulated interface can expand Landau levels into magnetic minibands, but our calculation reveals that the broadening of the miniband where the Fermi level is located is small and negligible for the density $n_e=3.9\times10^{11}$ cm^{-2}. Therefore, the quenching of the odd-integer quantum Hall effect observed experimentally[6] cannot be explained by the miniband broadening due to the periodic interface modulation.

A high anisotropy of the electron mobility has been observed.[5,6] Experiments show that the longitudinal mobility parallel to the quantum-wire direction is much larger than the transverse mobility. The present calculation gives an almost circular and isotropic Fermi line for the usual electron density and therefore shows that Bragg reflection due to the

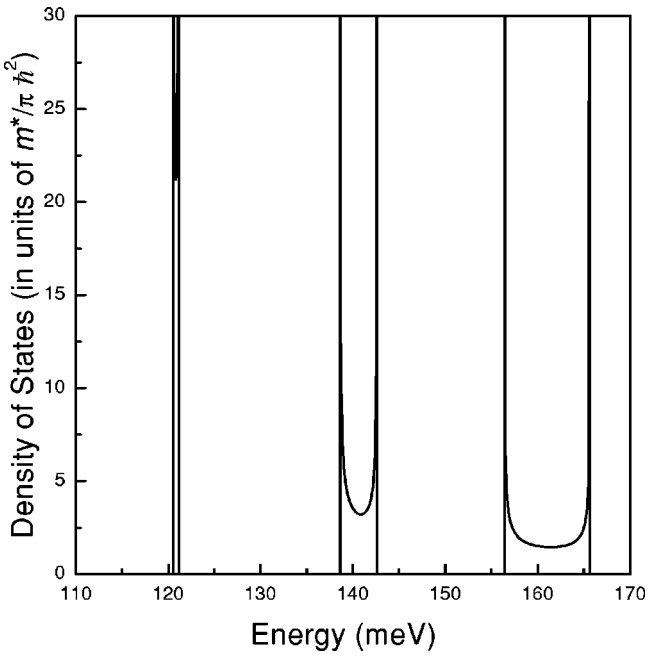

FIG. 8. The density of states in a magnetic field. Only the lowest three magnetic minibands are shown. The parameters take the values as $d_1=5$ nm, $a=12$ nm, $a_1=4$ nm, $\Delta=1.2$ nm, and $d=20$ nm. The magnetic field strength is $\hbar\omega_c=20$ meV or $B=11.57$ T.

periodic variation of the well thickness cannot give rise to considerable effects on the electron mobility.

A QWA structure was implemented also in a $GaAs/Al_xGa_{1-x}As$ single heterostructure where a large mobility anisotropy was also observed.[22] It is straightforward to develop a one-dimensional effective-potential model by

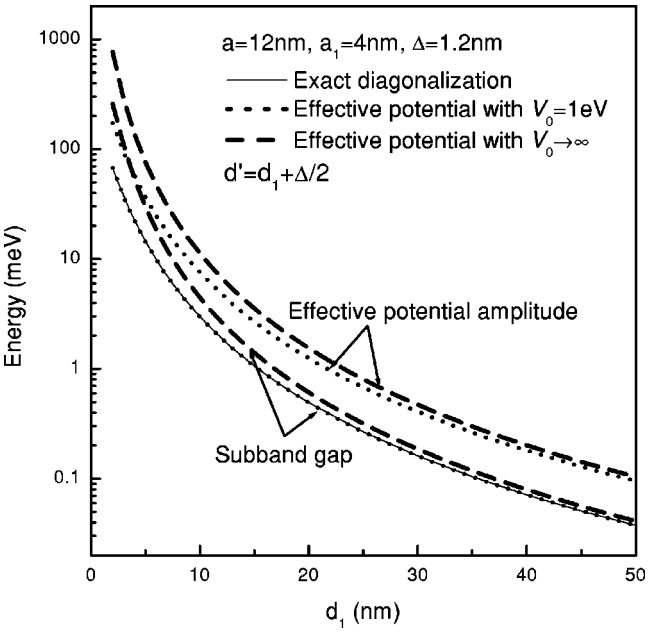

FIG. 9. Subband gaps between the first and second subbands calculated by different schemes and the amplitude of the effective potential ΔV as functions of the parameter d_1.

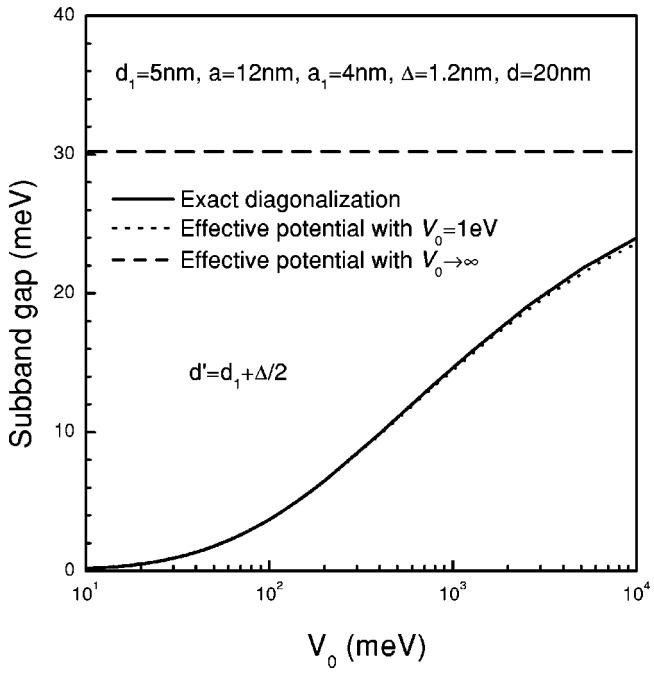

FIG. 10. The subband gaps as a function of V_0 calculated for actual QWA's and in the effective-potential scheme.

treating the periodic interface-position modulation as a periodic interface roughness in such single heterostructures.[23] The band offset of the $GaAs/Al_xGa_{1-x}As$ heterointerface depends on the Al concentration x as $V_0=0.6\times(1.155x+0.37x^2)$ eV for $x\leqslant 0.45$.[14,15] Thus the height of $GaAs/Al_xGa_{1-x}As$ quantum well is much smaller than that of the GaAs/AlAs quantum well ($V_0\approx 357$ meV for $x=0.45$). Therefore, the deviation of the band structure from that of the uniform 2D system is expected to be almost negligible in this system also. The anisotropy of the mobility cannot be ascribed to band-structure effects and is likely to be due to other more significant effects such as possible inhomogeneity and disorder in the periodic well-width variation.

V. SUMMARY

We have calculated the energy spectrum of a quantum-wire-array structure. In the absence of a magnetic field, only the lowest subband is partially occupied at the low-temperature limit in the case of typical electron density of experimental samples. Only in a quantum-wire array as thin as 2 nm, the subband can show a notable deviation from the parabolic band in the energy range from the subband bottom to the Fermi energy. In systems as thick as 5 nm (so far most experimental samples have thickness close to or larger than 5 nm), such a deviation is negligible. This implies that the modulation of the periodic potential due to interface corrugation does not play an important role in transport properties. When a high magnetic field is applied, the Landau levels are expanded into magnetic minibands which are a periodic function of the wave vector q_y. However, the broadening is still small and the Landau level picture remains valid under usual experimental circumstances.

More importantly, we have developed a one-dimensional

effective-potential model treating the well-width variation as an interface roughness. This model can well reproduce the energy spectrum in both presence and absence of a magnetic field and provides a intuitive and simple picture to understand electronic states of a quantum-wire array.

ACKNOWLEDGMENTS

This work was supported in part by a Grant-in-Aid for COE Research (12CE2004 ''Control of Electrons by Quantum Dot Structures and Its Application to Advanced Electronics'') from Ministry of Education, Culture, Sports, Science, and Technology Japan. One of the authors (Y.Z.) would like to thank the Ministry for the provision of scholarship and acknowledge the National Science Foundation of China for the financial support under Grant Nos. NNSFC69890220 and NNSFC69971012. Numerical calculations were performed in part using the facilities of the Supercomputer Center, Institute for Solid State Physics, University of Tokyo.

[1] M. Higashiwaki, M. Yamamoto, T. Higuchi, S. Shimomura, A. Adachi, Y. Okamoto, N. Sano, and S. Hiyamizu, Jpn. J. Appl. Phys. **35**, L606 (1996).
[2] M. Yamamoto, M. Higashiwaki, S. Shimomura, N. Sano, and S. Hiyamizu, Jpn. J. Appl. Phys. **36**, 6285 (1997).
[3] M. Higashiwaki, K. Kuroyanagi, K. Fujita, N. Egami, S. Shimomura, and S. Hiyamizu, Solid State Electron. **42**, 1581 (1998).
[4] M. Higashiwaki, S. Shimomura, S. Hiyamizu, and S. Ikawa, Appl. Phys. Lett. **74**, 780 (1999).
[5] Y. Ohno, T. Kitada, S. Shimomura, and S. Hiyamizu, Jpn. J. Appl. Phys. **40**, L1058 (2001).
[6] Y. Iye, A. Endo, S. Katsumoto, Y. Ohno, S. Shimomura, and S. Hiyamizu, Physica E **12**, 200 (2002); *Proceedings of 10th International Conference on Narrow Gap Semiconductors* (unpublished).
[7] R. Kubo, S. J. Miyake, and N. Hashitsume, in *Solid State Physics*, edited by F. Seitz and D. Turnbull (Academic Press, New York, 1965), Vol. 17, p. 269.
[8] D.B. Chklovskii, B.I. Shklovskii, and L.I. Glazman, Phys. Rev. B **46**, 4026 (1992); **46**, 15606 (1992) [Erratum].
[9] D.B. Chklovskii, K.A. Matveev, and B.I. Shklovskii, Phys. Rev. B **47**, 12605 (1993).
[10] K. Lier and R.R. Gerhardts, Phys. Rev. B **50**, 7757 (1994).
[11] T. Suzuki and T. Ando, J. Phys. Soc. Jpn. **62**, 2986 (1993); Physica B **201**, 345 (1994); **227**, 47 (1996); **249-51**, 415 (1998).
[12] S. Mori and T. Ando, J. Phys. Soc. Jpn. **48**, 865 (1980).
[13] For details on interface roughness, see, for example, T. Ando, A.B. Fowler, and F. Stern, Rev. Mod. Phys. **54**, 437 (1982).
[14] H.J. Lee, L.Y. Juravel, J.C. Woolley, and A.J. Springthorpe, Phys. Rev. B **21**, 659 (1980).
[15] G.D. Sanders and K.K. Bajaj, Phys. Rev. B **36**, 4849 (1987).
[16] M.H. Meynadier, C. Delalande, G. Bastard, M. Voos, F. Alexandre, and J.L. Liévin, Phys. Rev. B **31**, 5539 (1985).
[17] J.B. Xia, Phys. Rev. B **38**, 8358 (1988).
[18] S. Adachi, J. Appl. Phys. **58**, R1 (1985).
[19] M.J. Snelling, G.P. Flinn, A.S. Plaut, R.T. Harley, A.C. Tropper, R. Eccleston, and C.C. Phillips, Phys. Rev. B **44**, 11345 (1991).
[20] T. Ando and Y. Uemura, J. Phys. Soc. Jpn. **37**, 1044 (1974).
[21] A. Manolescu and R.R. Gerhardts, Phys. Rev. B **51**, 1703 (1995).
[22] Y. Nakamura, T. Noda, J. Motohisa, and H. Sakaki, Physica E **8**, 219 (2000).
[23] T. Ando, J. Phys. Soc. Jpn. **51**, 3900 (1982).